

Manganese Antimonate: Facile solid state synthesis, characterization and its application for Biginelli reactions

S. Khademinia¹, M. Behzad^{2*}, M. Rahimkhani³

¹Assistant Professor, Department of Chemistry, Semnan University, Semnan 35351-19111, Iran

²Associate Professor, Department of Chemistry, Semnan University, Semnan 35351-19111, Iran

³PhD Student, Faculty of physics, Semnan University, Semnan 35131-19111, Iran

* Corresponding author's E-mail: mbehzad@semnan.ac.ir

ABSTRACT

Nanostructured $Mn_2Sb_2O_7$ powders were synthesized via stoichiometric 1:1 Mn:Sb molar ratio solid state reaction at different reactions temperatures for 8 h using $MnSO_4 \cdot H_2O$ and Sb_2O_3 as raw materials. The synthesized materials were characterized by powder X-ray diffraction (PXRD) technique. Structural analyses were performed by the *FullProf* program employing profile matching with constant scale factors. The results showed that the patterns had a main monoclinic $Mn_2Sb_2O_7$ crystal structure with space group $P2_1$. The morphologies of the synthesized materials were studied by field emission scanning electron microscopy (FESEM) and Transmission electron microscopy (TEM) which showed that the $Mn_2Sb_2O_7$ samples had flower like and spherical particles morphologies. Ultraviolet – Visible spectroscopy (UV-Vis) showed that the band gap was about 2.85 eV. The most pure sample (S_6) was used as catalyst in the one-pot synthesis of the heterocyclic compounds 3,4-dihydropyrimidin-2(1H)-ones (DHPMs) in Biginelli reactions. Experimental design was used to find the optimized reaction conditions.

Keywords: Solid state reaction, FullProf, Pyrochlore, Nanocatalyst, Biginelli

1. INTRODUCTION

The ideal $A_2B_2O_7$ pyrochlore structure is commonly described as a derivative of the fluorite structure with space group $Fd\bar{3}m$ [1]. Pyrochlores are refractory materials with important properties, including ionic conductivity [2-4], optical nonlinearity [5], high radiation tolerance [6] and heat capacity [7]. They have many potential

applications, including thermal barrier coatings [8], dielectrics [9-11], solid electrolytes in solid-oxide fuel cells, [12] materials for safe disposal of actinide-containing nuclear wastes [13-16], photocatalyst [17] and p or n-type semiconductor [18]. Among them, $A_2Sb_2O_7$ compounds have found potential ferroelectric and/or magnetic applications. Three structures have been previously found for $A_2Sb_2O_7$

type compounds: i) the cubic pyrochlore (e.g. $\text{Pb}_2\text{Sb}_2\text{O}_7$), ii) the orthorhombic weberite (e.g. $\text{Sr}_2\text{Sb}_2\text{O}_7$, $\text{Ca}_2\text{Sb}_2\text{O}_7$), and iii) the trigonal weberite (e.g. $\text{Mn}_2\text{Sb}_2\text{O}_7$). Trigonal $\text{Mn}_2\text{Sb}_2\text{O}_7$ was first obtained by high-temperature solid state reaction and was described as a rhombohedrically distorted pyrochlore [19] but was later proved to be a weberite structure [20]. The Mn–Sb–O system contains a limited number of known compounds, namely MnSb_2O_4 and $\text{Mn}_3\text{Sb}_2\text{O}_6$ with trivalent antimony (JCPDS card 20-702), and MnSb_2O_6 and $\text{Mn}_2\text{Sb}_2\text{O}_7$ with pentavalent antimony. $\text{Mn}_2\text{Sb}_2\text{O}_7$ also adopts a structure different from that of other $\text{M}_2\text{Sb}_2\text{O}_7$ compounds with weberite or pyrochlore structure when synthesized at high-temperature [21]. Pyrochlore-type $\text{Mn}_2\text{Sb}_2\text{O}_7$ is only stable at temperatures below 600 °C [22]. Cubic $\text{Mn}_2\text{Sb}_2\text{O}_7$ pyrochlore could be obtained through a low temperature solid state reaction [23], high temperature solid state reaction [24, 25], and calcinations at different temperatures [26].

The Biginelli reaction was originally reported by Biginelli in 1891 [27]. It is a methodology for the synthesis of 3,4-dihydropyrimidin-2-(1H)-one derivatives (DHPMs) in a one-step procedure. DHPMs have shown several activities [28]. Several metal oxides have been reported as nanocatalysts for the Biginelli reactions [29-37]. In the present study, solid state reactions were explored for the synthesis of nanostructured $\text{Mn}_2\text{Sb}_2\text{O}_7$. $\text{MnSO}_4 \cdot \text{H}_2\text{O}$ and Sb_2O_3 were used as raw materials. Morphologies and particle size distributions of the as-prepared $\text{Mn}_2\text{Sb}_2\text{O}_7$ nanomaterials were studied by FESEM and TEM techniques. The band gap energy was estimated from UV-Vis spectrum. Textural properties of the compound were also studied by BET [38] and BJH [39] methods. The most pure sample was used as

nanocatalyst in Biginelli reaction for the synthesis of various DHPMs. It was found that the synthesized nanocatalyst had excellent efficiency in the synthesis of DHPMs. It should be noticed that in Biginelli reaction, not only do the type and amount of a catalyst influence the efficiency of the reaction, but also the amount of the analyte, temperature and reaction time are important factors which must be optimized. The common method to optimize these factors is one-factor-at-a time method (OFAT) varying one factor at a time while keeping all others fixed. However, experimental design method [40, 41] which varies several factors simultaneously is more efficient when studying two or more factors. Compared to OFAT method, this optimization methodology is preferred because of saving in time and cost (less number of experiment) for information achieved. Moreover the effects of each factor are estimated more precisely. To the best of our knowledge there are very rare reports about application of experimental design to optimize this reaction [37]. In this purpose, combination of two level full factorial design with some replicate centre points and response surface methodology [42] was applied.

2. EXPERIMENTAL

2.1. General remarks

All chemicals were of analytical grade and used without further purification. Phase identifications were performed on a powder X-ray diffractometer D5000 (Siemens AG, Munich, Germany) using $\text{CuK}\alpha$ radiation. SEM images were obtained on a field emission scanning electron microscope (Hitachi FE-SEM model S-4160). $\text{Mn}_2\text{Sb}_2\text{O}_7$ particles were dispersed in water and cast onto a copper grid to study the sizes and morphology of the particles by TEM (Transmission

Electron Microscopy) using a Philips – CM300 - 150 KV microscope. The average particle size distribution was carried out using Image software. Absorption and photoluminescence spectra were recorded on a Analytik Jena Specord 40 (Analytik Jena AG Analytical Instrumentation, Jena, Germany) and a Perkin Elmer LF-5 spectrometer (Perkin Elmer Inc., Waltham, MA, USA), respectively. The textural properties were analyzed using the Brunauer-Emmett-Teller (BET) and Barrett-Joyner-Halenda (BJH) methods on a Beckman Coulter SA3100 Surface Area Analyzer. The purity of the DHPMs was checked by thin layer chromatography (TLC) on glass plates coated with silica gel 60 F254 using n-hexane/ethyl acetate mixture as mobile phase.

2.2. Synthesis of $Mn_2Sb_2O_7$ nanomaterials

In typical synthetic experiments, 0.50 g (2.96 mmol) of $MnSO_4 \cdot H_2O$ ($M_w = 168.94 \text{ g mol}^{-1}$) and 0.43 g (1.48 mmol) of Sb_2O_3 ($MW = 291.5 \text{ g mol}^{-1}$) were mixed in a mortar and ground until a nearly homogeneous powder was obtained. The obtained powder was added into a 25 mL crucible and treated thermally in one step at 450 °C (S_1), 550 °C (S_2), 550 °C and then reground and heated at 450 °C (S_3), 550 °C and then reground and heated at 550 °C (S_4), 650 °C (S_5) and 750 °C (S_6) for 8 h. The crucible was then cooled normally in oven to the room temperature. The obtained powder was collected for further analyses. The synthesis yield ($MW = 465.48 \text{ g mol}^{-1}$) was 0.66 g (94%) for S_6 .

2.3. General procedure for the synthesis of DHPMs

In a typical procedure, a mixture of aldehyde (1 mmol), ethyl/methyl-acetoacetate (1 mmol), urea (1.2 mmol)

and 0.04 g of S_6 as catalyst were placed in a round-bottom flask under solvent free conditions. The suspension was stirred at 103 °C. The reaction was monitored by thin layer chromatography (TLC) [6:4 hexane:ethylacetate]. After completion of the reaction, the solid crude product was washed with deionized water to separate the unreacted raw materials. The precipitated solid was then collected and dissolved in ethanol to separate the solid catalyst. The filtrate was evaporated to dryness to obtain the pure DHPM.

3. RESULTS AND DISCUSSION

3.1. PXRD analysis

The phase composition of $Mn_2Sb_2O_7$ nanomaterials were examined by powder X-ray diffraction technique. Figure 1(a-f) shows the PXRD patterns of the obtained materials in the 2θ range 10-90° as well as the structural analyses performed by the *FullProf* program. The structural analyses were performed employing profile matching with constant scale factors. Red lines are the observed intensities; the black ones are the calculated data; the blue ones are the difference: $Y_{obs} - Y_{calc}$; and the Bragg reflections positions are indicated by blue, red and green bars for $Mn_2Sb_2O_7$, SbO_2 and Sb_2O_3 respectively. The patterns have well fitted defect pyrochlore structure profile with monoclinic structure. The results showed that the pattern had a main $Mn_2Sb_2O_7$ crystal structure with space group $P2_1$ [43]. Besides, it was found that there were small amounts of SbO_2 and Sb_2O_3 [44] as impurity which were crystalized in orthorhombic crystal structure with the space groups of $Pna21$ and $P2_1/c$, respectively. Table 1 shows the interplanar spacing (d) data calculated from Bragg's equation for $Mn_2Sb_2O_7$ nanomaterials. It was found that the d values were

nearly constant with increasing the reaction temperatures.

Table 1. Interplanar spacing (d) data for Mn₂Sb₂O₇ nanomaterials.

	S ₁	S ₂	S ₃	S ₄	S ₅	S ₆
d (Å)	3.1247	3.1164	3.1102	3.1452	3.0845	3.1259
2θ	28.5317	28.6097	28.6681	28.3420	28.9118	28.5211

Table 2 shows the crystal sizes of the obtained nanomaterials in different reaction temperatures calculated via Scherrer equation: $D = \frac{k\lambda}{\beta \cos \theta}$. In this equation, D(nm) is the entire thickness of the crystalline sample, λ is the X-ray diffraction wavelength (0.154 nm), and k is the Scherrer constant (0.9), β of FWHM is the full width at half its maximum intensity and h is the half

diffraction angle at which the peak is located. The data mentioned in table 2 show that with increasing the reaction temperature, the crystal sizes were increased from S₁ to S₃. The crystal size of S₆ was also increased due to the temperature increase but a slight decrease was observed for S₄ and S₅.

Table 2. Scherrer data information for Mn₂Sb₂O₇ nanomaterials.

Data	2θ	θ	B _{1/2} (°)	B _{1/2} (rad)	cosθ _B	Crystal size (nm)
S ₁	28.53	14.27	0.33216	0.00586816	0.969	24.4
S ₂	28.61	14.30	0.32905	0.00574002	0.969	24.9
S ₃	28.67	14.33	0.23142	0.00403699	0.969	35.4
S ₄	28.34	14.17	0.29346	0.00511924	0.970	27.9
S ₅	28.91	14.46	0.30158	0.00526089	0.968	27.2
S ₆	28.52	14.26	0.21331	0.00372107	0.969	38.4

The quantitative phase analysis was investigated with direct comparison method. In the method, we compared the experimental line intensity of the impurity phases (SbO₂, MnO₂ and Sb₂O₃) from the mixture to a line from the main phase (Mn₂Sb₂O₇) in the mixture. For this purpose, we chose the peaks with highest intensity for each phase at about 28.9°, 19.8° and 23.9° for Mn₂Sb₂O₇, SbO₂ and Sb₂O₃,

respectively. The phase comparison values are summarized in table 3. Table 3 shows that with increasing the reaction temperature, the phase purity was improved. As could be seen from table 3, by increasing the reaction temperatures to 650 and 750 °C, the Sb₂O₃/Mn₂Sb₂O₇ was 0 and SbO₂/Mn₂Sb₂O₇ was decreased to 6 %.

Table 3. Quantitative phase analysis for the obtained nanomaterials.

Sample	Phase ratio (%)	
	SbO ₂ /Mn ₂ Sb ₂ O ₇	Sb ₂ O ₃ /Mn ₂ Sb ₂ O ₇
S ₁	13.0	14.2
S ₂	11.6	11.6
S ₃	10.6	10.2
S ₄	9.2	9.2
S ₅	12.6	10.7
S ₆	6.3	-

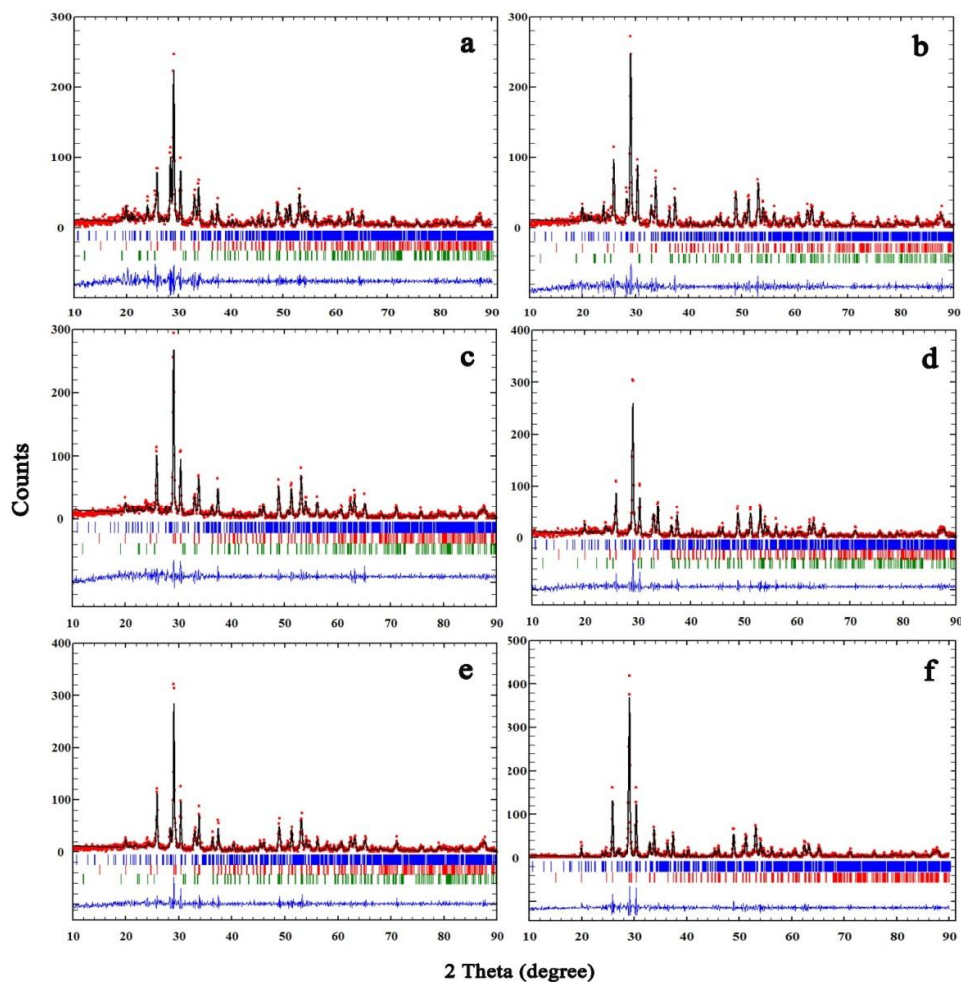


Fig. 1. PXRD pattern of the synthesized Mn₂Sb₂O₇ nanomaterials and the rietveld analyses. Where (a) is S₁, (b) is S₂, (c) is S₃, (d) is S₄, (e) is S₅ and (f) is S₆.

Table 4 shows the cell parameters data for Mn₂Sb₂O₇ obtained by rietveld analysis. It was found that with changing the reaction temperature, the cell parameters were nearly constant.

Besides, the table shows the R_f, Bragg R_b factors and χ^2 to show the goodness of the fittings.

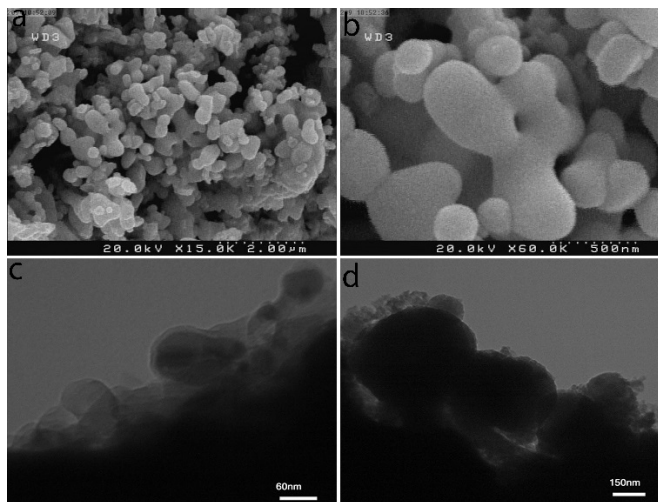
Table 4. Cell parameter data for the obtained $\text{Mn}_2\text{Sb}_2\text{O}_7$ nanomaterials

Sample	Cell parameters (Å)				R_f	R_b	X^2
	a	b	c	β			
S_1	5.440018	12.499397	8.280566	91.70	2.02	1.05	1.41
S_2	5.252693	12.534166	8.150705	91.60	2.29	1.29	1.51
S_3	5.352578	12.522385	8.344703	91.60	1.77	1.16	1.59
S_4	5.342128	12.570947	8.262301	91.50	1.99	1.24	1.50
S_5	5.170033	12.441152	8.135438	91.50	2.23	1.16	1.48
S_6	5.360686	12.506569	8.341183	91.50	2.19	1.21	1.55

3.2. Microstructure analysis

Figures 2a and b with the magnifications of ($\times 15000$ and $\times 60000$, respectively) show the FESEM images of S_6 as an example. These figures show that the morphology of the material was mainly porous type. The TEM images for S_6 are shown in figures 2c and d, respectively. As could be seen from the figure, the material is mainly consisted of spherical particles.

It also indicates that the particle sizes are in the range of 50 – 300 nm. TEM images show that probably one of the products such as $\text{Mn}_2\text{Sb}_2\text{O}_7$ play role of a matrix and the impurity compound have located on the surface of matrix. The particle size of matrix is ~ 300 nm and nanoparticle on the matrix is ~ 50 nm.

**Fig. 2.** FESEM and TEM images of S_6 .

3.3. BET and BJH texture analysis

The synthesized powders were characterized for their surface area, average pore size and average pore volume. Prior to N_2 -physical adsorption measurements, the samples were degassed at 150°C for 120 min in the nitrogen atmosphere. The specific surface area (S_{BET}) of the material was

determined with adsorption-desorption isotherms of N_2 at 77 K. The surface area, pore volumes and average pore diameters are summarized in table 5. From table 5, it could be seen that the surface area and pore volumes are about $115.0 \text{ m}^2\text{g}^{-1}$ and $0.22 \text{ cm}^3\text{g}^{-1}$, respectively. The average nanoparticle size was also measured as 52 nm. Table 6 also shows the textural properties of

the as-prepared material obtained from the BJH method. The high surface area and porous structure of the synthesized nanomaterial is confirmed by this analysis. It suggests that the

synthesized material could be a suitable candidate for special catalytic or other applications.

Table 5. BET data for $Mn_2Sb_2O_7$ showing the textural properties of the obtained material.

Property	Value
Surface Area	115.0 m ² /g
pore volume	0.22 cm ³ /g
average pore width	78 Å
Average Particle Size	52 nm

Table 6. BJH data for $Mn_2Sb_2O_7$ showing the textural properties of the obtained material.

Property	Value
BJH desorption cumulative surface area of pores between 17 and 3000Å width	177.7 m ² /g
BJH desorption cumulative volume of pores between 17 and 3000Å width	0.23 cm ³ /g
BJH desorption average pore width (4V/A)	53 Å

3.4. Optical properties

Figure 3 shows the photoluminescence (pL) emission spectrum which was carried out by excitation wavelength of 450 nm. This figure displays a broad and strong emission band peaked at 650 - 700 nm. The broad and intensive peak in figure 3 is indicative of the oxygen deficiency in the crystal structure which is typical of the $A_2B_2O_7$ pyrochlores.

Figures 4a and b show the UV-Vis spectrum and band gap energy plot for S_6 . Our literature survey showed that there was no report on the optical properties of the $Mn_2Sb_2O_7$ nanomaterial. UV-Vis absorption spectrum of the as-prepared $Mn_2Sb_2O_7$ nanomaterial is shown in

figure 4a. A plot of $(ahv)^2$ versus hv (eV) is also shown in figure 4b as well as the calculated direct band gap energies. The pure $Mn_2Sb_2O_7$ nanomaterial displays typical visible absorption edge at about 420 and 580 nm. According to the results of Pascual et al. [45], the relation between the absorption coefficient and incident photon energy can be written as $(\alpha hv)^2 = A(hv - E_g)$, where A and E_g are a constant and direct band gap energy, respectively. Band gap energy was evaluated by extrapolating the linear part of the curve to the energy axis. It was found that the band gap was about 2.85 eV.

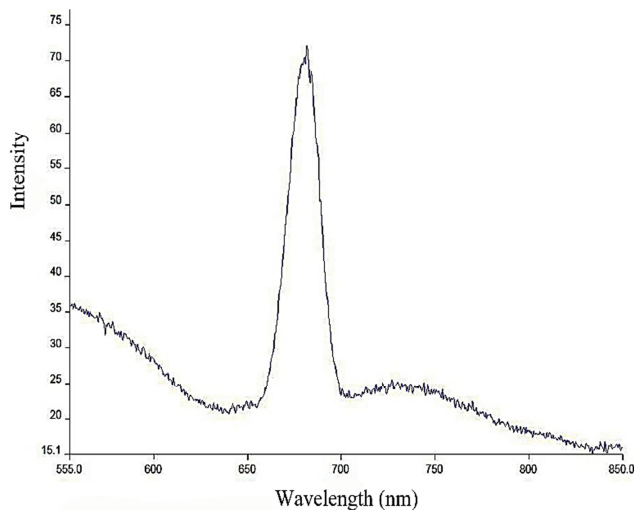


Fig. 3. Photoluminescence emission spectrum for S_6 ($\lambda_{ex}=450$ nm).

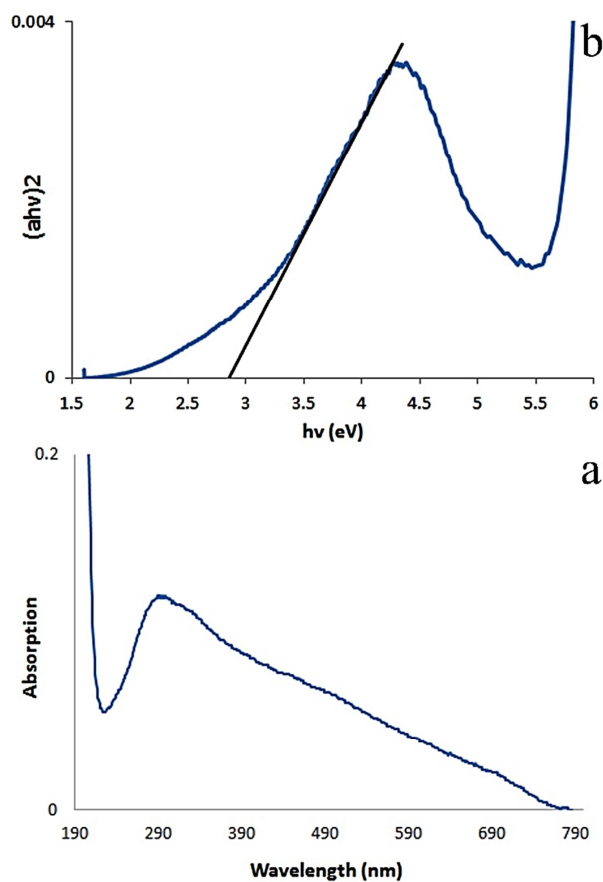


Fig. 4. Plots of a) UV-Vis spectrum and b) $(ahv)^2$ versus $h\nu$ (eV) for S_6 .

3.5. Catalytic studies

3.5.1. Experimental design and achieving optimal conditions in Biginelli reactions

There are different kinds of experimental designs in the literature for exploring the optimal level of the factors affecting a chemical reaction. Full factorial design [40, 41] is one of

the common method defined by all possible combinations of the factors and their settings. Imagine that there are k investigating factors and there are m different levels for each factor. All possible combinations of the factors and their settings will then be m^k . In chemical processes, two-level factor setting is prevalent since such designs allow the determination of all main effects and all interaction effects with small number of experiment.

The relation between factors and response can be theoretically modeled by a function which is the underlying physical mechanism to the problem under study. This relation makes the reproducibility in the system under investigation to be able to experiment with it and to interpret the results. Response surface methodology (RSM) is a mathematical and statistical method, which applies an empirical model to analyze experimental design data [42].

The adequacy of the applied model is verified by analysis of variance (ANOVA) [46] requiring some replicate experiments.

In this study, the goal was to find the optimum amount of the nanocatalyst, temperature and time for the Biginelli reaction by monitoring the kinetic reaction at different conditions. Different possible combinations of these factors were designed which reported in table 7 and the yield % of the reaction was obtained as response. Here, some axillary points were included in the design: four replicates at the center of factors for the validation of the model by ANOVA and four points to obtain more robust models. All the experiments were carried out at two days with random order.

The observed data of the factorial design was fitted to a linear response model. First, low and high factor levels were coded to -1 and +1, respectively,

and then the model is applied. Equation 1 expresses the relation between the factors and the yield of the reaction, $Y\%$, based on the first order model combined with some two-factor interaction terms:

$$Y\% = 41.33 + 5.06 X_1 + 37.32 X_2 + 4.7 X_3 + 6.4 X_{12} + 3.84 X_{23} \quad (\text{Equation 1})$$

X_1 , X_2 and X_3 are the amount of the catalyst, temperature and time of the reaction respectively. X_{12} and X_{23} are the interaction terms between X_1 and X_2 ; and X_2 and X_3 , respectively. This equation reveals that are not only the main factors: X_1 , X_2 and X_3 important, but also the interaction effects of the amount of catalyst and temperature (X_1 and X_2 , respectively); and time and temperature (X_2 and X_3 , respectively) are significant. Therefore, to optimize the reaction condition, all of these parameters must be considered. It should be noticed that the more the value of the parameters is, the more the effect is. Here, the effect of the temperature is the highest one, next, the interaction between the amount of the catalyst and temperature is the highest effect among the others. Also, the effect of the catalyst and time are approximately equal.

The ANOVA results reported in table 8 show that the p -value of the regression was smaller than 0.05, revealing that the model was significant at a high confidence level (95%) [42]. The p -value probability of lack of fit was greater than 0.05, which verified the models' significance. Also the coefficients of determination consist of R -square, adjusted- R -square and R^2 -pred were used to present the quality of fit of polynomial model equation. In this case, R^2 of variation fitting for $Y\%$ 0.9738 indicated a high degree of correlation between the response and the independent factors. Also, the high value of regression coefficient R^2 -adj = 0.9592 and R^2 -pred = 0.8213 verify the

high prediction power of the suggested model.

To depict the effects in the above model, the three-dimensional (3D) response surfaces plot of the response,

using equation (1) when one factor value was fixed at optimum level and the other two were varied is shown in figure 5.

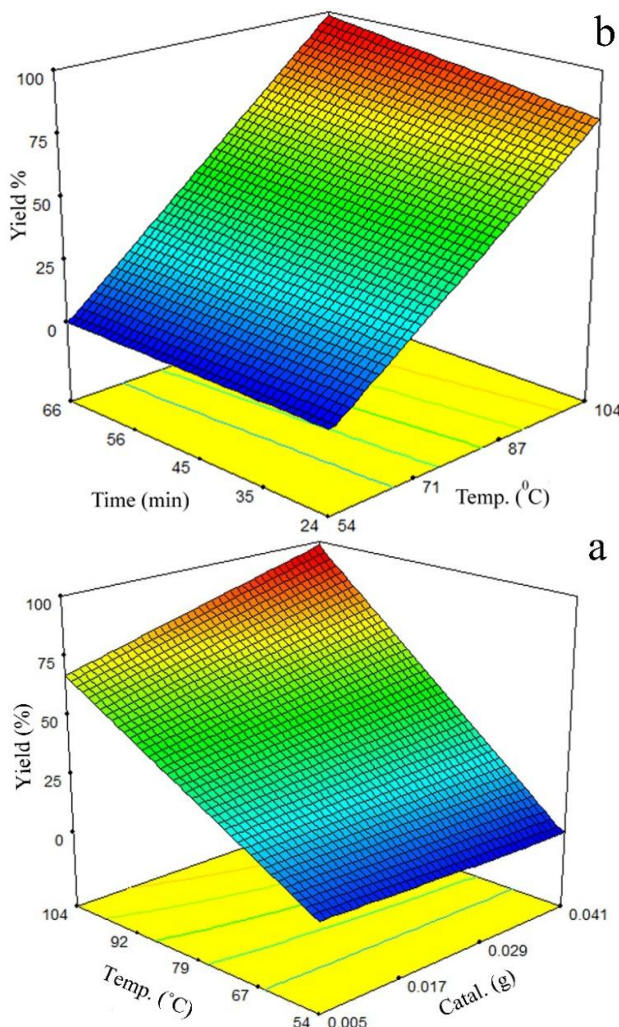


Fig. 5. Illustration of 3D plot of the response surface of Biginelli reaction yield

The goal of the optimization was to find the condition in which the yield of the reaction is maximized. The results indicated that 0.040 g of the catalyst, 103 °C reaction temperatures, and 62 min reaction time were the optimum parameters for the synthesis of DHPMs. Briefly, applying intelligent experimental design and RSM helped us to find accurate optimal condition because,

in this reaction, apart from the main effects, the interaction effects were significant. Moreover, the importance of factors and their interactions were quantified and the factor effects on the reaction were depicted and interpreted. The optimized parameters were used for the synthesis of other derivatives and the results were collected in table 9.

Table 7. Two-level full factorial design with some axillary points, in Biginelli reaction*

	Catalyst (g)	Temp (°C)	Time (min)	Yield (%)
day1	0.041	56	66	0
day1	0.014	56	24	0
day 1	0.028	80	45	50
day 1	0.014	104	66	81
day1	0.041	104	24	81
day 1	0.028	80	45	50
day 2	0.041	56	24	0
day 2	0.014	56	66	0
day 2	0.028	80	45	46
day 2	0.028	80	45	42
day 2	0.014	104	24	54
day 2	0.041	104	66	92
day 2	0.02	104	66	85
day 2	0.005	104	66	77
day 2	0.005	120	66	81
day2	0.005	104	66	77

* Benzaldehyde: ethylacetoacetat: urea molar ratios is as follows: 1:1:1.2

Table 8. Analysis of variance for the suggested model *

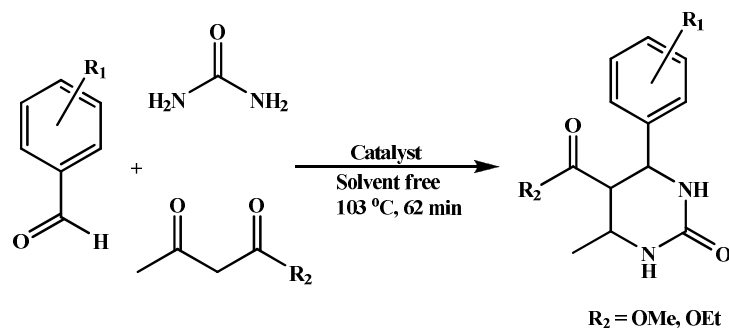
Source	DF	SS	F	P
Block	1	1382.4		
Regression	5	15607.53	66.88	<0.0001
Residual error	9	420.07		
Lack-of-fit	7	412.07	14.72	0.0651
Pure error	2	8.00		
Total	15	17410.0		

*For detailed explanation of the table, refer to [46].

3.5.2. Biginelli reaction for the synthesis of DHPMs

The one pot condensation between ketoesters, aldehyde and urea, in the presence of either Lewis or mineral acids results in the synthesis of DHPMs. In this study, DHPMs were

prepared from the condensation of aromatic aldehydes, ethyl acetoacetate and used in presence of 0.04 g of S₆ at 103 °C for 62 min under solvent free conditions (scheme 1). The results are collected in Table 9.



Scheme 1. Schematic representation of the reaction pathway for the synthesis of DHPMs.

Table 9. Biginelli reactions using ethyl/methyl acetoacetate and urea with different benzaldehyde derivatives.

R ₁	R ₂	Yield (%)
H	OEt	81
4- Cl	OEt	92
2- Cl	OEt	77
4- Br	OEt	96
4- F	OEt	19
3-NO ₂	OEt	100
2- OMe	OEt	58
3-OMe	OEt	46
3-OH	OEt	54
4-OH	OEt	46
3,4-OH	OEt	54
H	OMe	85
4- Cl	OMe	85
2- Cl	OMe	73
4- Br	OMe	96
4- F	OMe	23
3-NO ₂	OMe	85
2- OMe	OMe	46
3-OMe	OMe	54
3-OH	OMe	38
4-OH	OMe	42
3,4-OH	OMe	46

To show the merit of the present work, we have compared the as synthesized $\text{Mn}_2\text{Sb}_2\text{O}_7$ nanocatalyst results with some of the previously reported catalysts in the synthesis of

DHPMs (table 10). It is clear that the synthesized $\text{Mn}_2\text{Sb}_2\text{O}_7$ nanocatalyst showed greater activity than some other heterogeneous catalysts.

Table 10. Comparison study of the catalytic ability of the synthesized $\text{Mn}_2\text{Sb}_2\text{O}_7$ nanocatalyst with other catalysts.

Catalyst	R ₁	Catalyst amount	Reaction Condition	Yield %	Time (min)	Ref.
S ₆	H	0.04 g	solvent-free, 103 °C	81	62	This work
	4-Cl			92		
	2-Cl			77		
Bi ₂ V ₂ O ₇	H	3.1 × 10 ⁻² mmol	solvent-free, 90 °C	89	60	[29]
	4-Cl			92		
	2-Cl			98		
ZrO ₂ -Al ₂ O ₃ -Fe ₃ O ₄	H	0.05 g	Ethanol, reflux, 140 °C	82	300	[30]
	4-Cl			66		
	2-Cl			40		
Mo/γ - Al ₂ O ₃	H	0.3 g	solvent-free conditions at 100 °C	80	60	[32]
ZnO	H	25 mol%	solvent-free conditions at 90 °C	92	50	[33]
	4-Cl			95		
Bi ₂ O ₃ /ZrO ₂	H	20 mol%	solvent-free, 80-85 °C	85	120	[34]
	4-Cl			85	120	
	2-Cl			82	165	
Bi ₂ Mn ₂ O ₇	H	2.2 × 10 ⁻² mmol	solvent-free, 104 °C	96	66	[37]
	4-Cl			89		
	2-Cl			86		

3.5.3. Reusability of the catalyst

For practical applications of this heterogeneous catalyst the level of reusability was also tested. The

recycled catalyst could be reused for at least three times with small decrease in yield (Figure 6).



Fig. 6. Reusability of $\text{Mn}_2\text{Sb}_2\text{O}_7$ in Biginelli reaction.

4. CONCLUSION

In this his work, $Mn_2Sb_2O_7$ nanomaterials were synthesized via solid state method. PXRD patterns and structural analysis were performed by FullProf program employing profile matching. The data showed that the syntheses were successful and the patterns had a main $Mn_2Sb_2O_7$ crystal structure with space group $P2_1$. FESEM and TEM images showed sphere-like morphology in the as-synthesized materials. Direct band gap energy of about 2.85 eV was obtained for S_6 . The catalytic application of the synthesized nanomaterial (S_6) was investigated in Biginelli reaction in solvent free conditions. It was found that $Mn_2Sb_2O_7$ nanomaterial had excellent efficiency in the synthesis of DHPMs. Besides, the two metal ions have performed the catalytic reactions cooperatively.

REFERENCES

- [1] H. Jiang, W. You, X. Liu, J. Liao, P. Wang, B. Yang, *B. Mater. Sci.*, 36, 1147 (2013).
- [2] M. B. Johnson, D. D. James, A. Bourque, H. A. Dabkowska, B. D. Gaulin, M. A. White, *J. Solid State Chem.*, 182, 725 (2009).
- [3] S. A. Kramer, H. L. Tuller, *Solid State Ion.*, 82, 15 (1995).
- [4] T. Norby, *J. Mater. Chem.*, 11, 11 (2001).
- [5] F. W. Shi, X. J. Meng, G. S. Wang, T. Lin, J. H. Ma, Y. W. Li, J. H. Chu, *Phys. B: Condens. Matter.*, 370, 277 (2005).
- [6] G. R. Lumpkin, M. Pruneda, S. Rios, K. L. Smith, K. Trachenko, K. R. Whittle, N. J. Zaluzec *J. Solid State Chem.*, 180, 1512 (2007).
- [7] Z. G. Liu, J. H. Ouyang, Y. Zhou, B. *Mater. Sci.*, 32, 603 (2009).
- [8] R. Vassen, D. Sebold, D. Stoeber, *Ceram. Eng. Sci. Proc.*, 28, 27 (2008).
- [9] W. Ren, S. Trolier-McKinstry, C. A. Randall, T. R. Shrout, *J. Appl. Phys.*, 89, 767 (2001).
- [10] S. G. Phadnis, R. Rajan, K. S. Kulkarni, B. *Mater. Sci.*, 2, 139 (1983).
- [11] K. Krishnankutty, K. R. Dayas, B. *Mater. Sci.*, 6, 907 (2008).
- [12] B. J. Wuensch, K. W. Eberman, C. Heremans, E. M. Ku, P. Onnerud, E. M. Yeo, S. M. Haile, J. K. Stalick, J. D. Jorgensen, *Solid State Ion.*, 129, 111 (2000).
- [13] R. C. Ewing, W. J. Weber, J. Lian, *J. Appl. Phys.*, 95, 5949 (2004).
- [14] K. R. Whittle, L. M. D. Cranswick, S. A. T. Redfern, I. P. Swainson and G. R. Lumpkin *J. Solid State Chem.*, 182, 442 (2009).
- [15] J. Hou, S. Jiao, H. Zhu, R.V. Kumar, *J. Solid State Chem.*, 184, 154 (2011).
- [16] M. Muthuraman, N. Arul Dhas, K. C. Patil, *B. Mater. Sci.*, 17, 977 (1994).
- [17] Z. S. Chen, W. P. Gong, T. F. Chen, S. L. Li, *B. Mater. Sci.*, 34, 429 (2011).
- [18] M. A. Subramanian, G. Aravamudan, G. V. Subba Rao, *B. Mater. Sci.*, 2, 201 (1980).
- [19] M. A. Subramanian, A. Clearfield, A. M. Umarji, G. K. Shenoy, G. V. Subba Rao, *J. Solid State Chem.*, 52, 124 (1984).
- [20] H. G. Scott, *Z. Kristallogr.*, 190, 41 (1990).
- [21] A. F. Wells, *Structural Inorganic Chemistry*, 5th Edition, Oxford University Press, Oxford (1984).
- [22] F. Brisse, D. J. Stewart, V. Seidl, O. Knop, *Can. J. Chem.*, 50, 3648 (1972).
- [23] H. D. Zhou, C. R. Wiebe, A. Harter, N. S. Dalal, J. S. Gardner, *J. Phys. Condens Matter.*, 20, 325201 (2008).
- [24] L. Chelazzi, T. B. Ballaran, G. O. Lepore, L. Bindi, P. Bonazzi, *Solid State Sci.*, 21, 85 (2013).
- [25] H. G. Scott, *J. Solid State Chem.*, 66, 171 (1987).
- [26] H. D. Zhou, C. R. Wiebe, J. A. Janik, B. Vogt, A. Harter, N. S. Dalal, J. S. Gardner, *J. Solid State Chem.*, 183, 890 (2010).

- [27] P. Biginelli, *Ber. Dtsch. Chem. Ges.*, 24, 1317 (1891).
- [28] K. Singh, D. Arora, S. Singh, *Mini Rev. Med. Chem.*, 9, 95 (2009).
- [29] S. Khademinia, M. Behzad, H.S. Jahromi, *RSC Adv.*, 5, 24313(2015).
- [30] A. Wang, X. Liu, Z. Su, H. Jing, *Catal. Sci. Technol.*, 4, 71 (2014).
- [31] J. Javidi, M. Esmailpour, F. N. Dodeji, *RSC Adv.*, 5, 308 (2015).
- [32] S. L. Jian, V. V. D. N. Prasad, B. Sain, *Cat. Com.*, 9, 499 (2008).
- [33] Kh. Pourshamsian. *Int. J. Nano Dimens.*, 6, 99 (2015).
- [34] J. Safari, S.G. Ravandi, *RSC Adv.*, 4, 11486 (2014).
- [35] J. Safari, S. G. Ravandi, *New J. Chem.*, 38, 3514 (2014).
- [36] J. Mondal, T. Sena, A. Bhaumik, *Dalton Trans.*, 41, 6173 (2012).
- [37] S. Khademinia, M. Behzad, A. Alemi, M. Dolatyari, S. M. Sajjadi, *RSC Adv.*, 5, 71109 (2015).
- [38] S. Brunauer, P. H. Emmett, E. Teller, *J. Am. Chem. Soc.*, 60, 309 (1938).
- [39] E. P. Barrett, L. G. Joyner, P. P. Halenda, *J. Am. Chem. Soc.*, 73, 373 (1951).
- [40] T. Lundstedt, E. Seifert, L. Abramo, B. Thelin, A. Nystrom, J. Pettersen, R. Bergman. *Chemometr. Intell. Lab.*, 42, 3 (1998).
- [41] R. Carlson, J. E. Carlson, *Design and Optimization in Organic Synthesis*; Elsevier: Amsterdam, (2005).
- [42] G. E. P. Box, N. R. Draper, *Empirical Model-Building and Response Surfaces*; Wiley: New York, (1987).
- [43] D. C Peets, H. Sim, M. Avdeev, *J. Physics: Conf. Series*. 807, 042002 (2017)
- [44] Z. Lei, L. P. Cheng, L. Yin, *Mater Lett.*, 75, 29 (2012).
- [45] J. Pascual, J. Camassel, M. Mathieu, *Phys. Rev. B: Solid State*, 18, 5606 (1978).
- [46] Comprehensive Chemometrics Chemical and Biochemical Data Analyses. Vol. 1, chapter 12, page 354 (2009).